Gene vectors based on DOEPC/DOPE mixed cationic liposomes: A Physicochemical Study

Mónica Muñoz-Úbeda,[1] Alberto Rodríguez-Pulido,[2] Aurora Nogales,[3] Oscar Llorca,[4] Manuel Quesada-Pérez,[5] Alberto Martín-Molina,[6] Emilio Aicart[1] and Elena Junquera[1,*]

[1]Grupo de Química Coloidal y Supramolecular, Departamento de Química Física I, Facultad de Ciencias Químicas, Universidad Complutense de Madrid, 28040-Madrid, Spain

[2]Department of Polymer Chemistry, Zernike Institute for Advanced Materials, University of Groningen, Nijenborgh 4, 9747 AG Groningen, The Netherlands.

[3]Instituto de Estructura de la Materia, CSIC, Serrano 121, 28006-Madrid, Spain

[4]Centro de Investigaciones Biológicas, CSIC, Ramiro de Maeztu 9, 28040-Madrid, Spain

[5] Departamento de Física, Escuela Politécnica Superior de Linares, Universidad de Jaén, 23700, Linares, Jaén, Spain.

[6]Grupo de Física de Fluidos y Biocoloides, Departamento de Física Aplicada, Facultad de Ciencias, Universidad de Granada, 18071-Granada, Spain

Corresponding author: E. Junquera

Tel: +34-913944131

Fax: +34-913944135

e-mail: junquera@quim.ucm.es

http://www.ucm.es/info/coloidal/index.html

*To whom correspondence should be addressed

Abstract

A double approach, experimental and theoretical, has been followed to characterize from a physicochemical standpoint the compaction process of DNA by means of cationic colloidal aggregates. The colloidal vectors are cationic liposomes constituted by a mixture of a cationic lipid, 1,2-dioleoyl-*sn*-glycero-3-ethylphosphocholine (chloride salt) (DOEPC) and a zwitterionic lipid, the 1,2-dioleoyl-sn-glycero-3-phosphatidylethanolamine (DOPE). A wide variety of high precission experimental techniques have been used to carry on the analysis: electrophoretic mobility, small-angle X-Ray diffraction or SAXS, cryogenic electron transmission microscopy or cryo-TEM and fluorescence spectroscopy (ethidium bromide intercalation assays). On the other hand, a theoretical model that considers the renormalization of charges of both the polyelectrolite and the colloidal aggregates shed light as well on the characteristics of the compaction process. This global information reveals that the compaction of DNA by the cationic liposomes is mostly driven by the strong electrostatic interaction among the positively charged surfaces of the colloidal aggregates and the negatively charged DNA, with a potent entropic component. DOEPC/DOPE liposomes are mostly spherical, with a mean diameter of around 100 nm and a bilayer thickness of 4.5 nm. From a morphological view point, an appreciable amount of multilamellar structures have been found not only on the lipoplexes but also on the parent liposomes. The isoneutrality of the lipoplexes is found at liposome/DNA mass ratios that decrease with the molar fraction of cationic lipid in the mixed liposome, α. This liposome composition has a clear effect as well on the lipoplex structure, which goes from an inverted hexagonal phase, H_{II}, usually related with improved cell transfection efficiency, at low cationic lipid molar fraction ($\alpha \approx 0.2$), to a lamellar structure, L_α, when the cationic lipid content on the mixed liposomes increases ($\alpha \geq 0.4$), irrespectively of the lipoplex charge ratio.

On the other hand, a theoretical complexation model is employed to determine the net charge of the lipoplexes studied in this work, by using renormalized charges. The model allows to confirm and predict the experimental isoneutrality conditions as well as to determine the maximum magnitude of this charge as a function of the composition of the resulting lipoplexes.

Introduction

In the last two decades, the interest in using synthetic non-viral vectors in gene delivery, as well as the publications from a large number of research groups, have dramatically increased.[1-11] One of the possible trails of this topic is based on the use of mixed lipids, constituted by a cationic and a zwitterionic lipids, to transfect genetic material forming what is known as lipoplexes.[4,11-17] The cationic lipid yields the positive charge to interact with both the negative delivery agent (i.e., DNA) and the negative cellular membranes, while the zwitterionic lipid is a helper lipid that decreases the toxicity of the cationic lipid, increases the fluidity of the mixed lipid bilayer, and makes the fusion with the plasmatic membrane easier, which finally drives to a better efficiency in gene therapy transfection.[1-8] Although the electrostatic interaction between cationic lipid and anionic DNA is expected to play a significant role in the lipoplex properties, it is necessary to increase the knowledge of this interaction not only from biochemical and chemical experiments but also from theoretical approaches.[6,11] It has been proved that a physicochemical study of the DNA compaction process by cationic lipids shed light in both the formation of the lipoplex and on the transfection mechanisms.[5,11,18] In this sense, the surface charge density and the mixed lipid composition, together with the lipoplex structure seem to be the main factors on the lipoplex transfection efficiency.[5,18] Thus, lipoplexes may form lamellar, hexagonal, or even cubic structures that interact with the cell membranes in different ways and effectiveness,[5,18] and the objective is to conjugate mixed lipids that form stable lipoplexes with DNA, together with an easy release of DNA into the cells within which they are expected to be as less cytotoxic as possible. Previous studies[5,12-14,17,18] have shown a direct relation between the different structures found in the lipoplexes and the lipidic composition of the liposome. Therefore, it is important to carry on a complete

study of the characteristics of novel lipoplexes at different lipid compositions, discovering the different structures developed by them and, accordingly, selecting the most promising vectors for gene therapy.

Due to its optimum properties as helper lipid, the 1,2-dioleoyl-sn-glycero-3-phosphoetanolamine (DOPE, see Scheme 1) is the most frequently used in transfection.[4,18-26] On the other hand, the 1,2-dioleoyl-*sn*-glycero-3-ethylphosphocholine (chloride salt) (DOEPC, see Scheme 1) is a cationic lipid that, at our knowledge, has never been studied as transfecting agent. Both lipids contain two identical hydrocarbon chains with an unsaturation on the *cis* configuration at the 9 position that, compared to the saturated hydrophobic chains, increases the fluidity of both bilayers and, obviously, of the mixed cationic-zwitterionic membranes used as vector in gene therapy. For all those reasons, we expect that the DOEPC/DOPE lipid mixture may be a potentially promising vector in gene therapy, and, accordingly, its physichochemical characterization in buffered solution in the absence (mixed liposomes) and the presence (lipoplexes) of DNA becomes very interesting. The study reported in this work has been carried out by means of several experiments: electrochemical methods, such as zeta potential, are a powerful tool to analyze the electrostatic interactions on the surface of the liposomes and/or the lipoplexes;[4,24,27-31] fluorescence ethidium bromide (EtBr) intercalation assays are used to check the DNA-liposome interaction, as well; [24,30,32-42] cryogenic electron transmission microscopy (cryo-TEM) experiments report information about the size, shape and morphology of mixed lipid vectors and lipoplexes,[19,23,24,43-49] while small angle X-ray scattering (SAXS) permits to determine the structure of the lipoplexes.[5,12-14,17,18] Furthermore, the compaction process of DNA by the cationic lipids has been also theoretically analyzed, by using the DNA complexation model developed by Nguyen and Shklovskii and later modified by

Sennato *et al.*[50-52] This theory was successfully employed in our previous works to study the phase diagrams of complexation of DNA with liposomes made of zwitterionic and cationic lipids.[16,17] However, the complexation model is employed at the present to determine the net charge of the lipoplexes studied in this work. In particular, the model allows to compare the maximum magnitude of this charge as a function of the composition of the resulting lipoplexes. Thus, the final objective of this work is to experimentally analyze and to theoretically predict the influence of the main factors that affect the DNA compaction process by mixed DOEPC/DOPE liposomes, as well as the characteristics of the resulting lipoplexes and their potential use on gene therapy.

Experimental Details

Materials. Cationic lipid, 1,2-dioleoyl-*sn*-glycero-3-ethylphosphocholine (chloride salt) (DOEPC), and zwitterionic lipid 1,2-dioleoyl-sn-glycero-3-phosphoetanolamine (DOPE), were from Avanti Polar Lipids. Sodium salt of calf thymus DNA (CT-DNA) was from Sigma-Aldrich. All of them, with the best purities, were used as supplied by the manufacturer. Solutions were prepared with distilled and deionized water (Super Q Millipore system, conductivity lower than 18 μS cm^{-1}), and all were buffered with PBS buffer at around physiological conditions (pH = 7.5 and ionic strength of 160 mM). A protocol widely explained elsewhere[15] was used for the preparation of mixed liposome and lipoplex solutions. A stock solution of CT-DNA was prepared two days before the mixing with liposomes. DNA concentrations (expressed in mM base pairs) were determined by absorbance at 260 nm (ε = 6600 M^{-1} cm)[53,54]. A A_{260}/A_{280} ratio of 1.90 and a negligible absorbance at 320 nm (A_{320} = -0.003) reveal[25,53-55] that the contamination of the DNA used in this work by the presence of a certain percentage of proteins is negligible.

Experimental Methods. The Phase Analysis Light Scattering technique (*Zeta PALS,* Brookhaven Instrum. Corp., USA) was used to measure electrophoretic mobilities (and from it, zeta potential) and particle sizes. This interferometric technique is up to 1000 times more sensitive than traditional light scattering methods based on the shifted frequency spectrum, and uses phase analysis light scattering to determine the electrophoretic mobility of charged colloidal suspensions. Each electrophoretic mobility data is taken as an average over 50 independent measurements. Electrophoretic mobility for liposome and lipoplex solutions was measured at each liposome composition (cationic to neutral lipid ratios) as a function of lipoplex compositions (liposome to DNA ratios).

Small-angle X-ray scattering (SAXS) experiments were carried out on a Bruker AXS nanostar small-angle X-ray scattering instrument. The instrument uses Cu KR radiation (1.54 Å) produced in a sealed tube. Samples were placed in sealed glass capillaries purchased from Hilgenberg with an outside diameter of 1.5 mm and wall thickness of 0.01 mm. The sample chamber is under vacuum. The scattered X-ray are detected on a two-dimensional multiwire area detector (Bruker Hi-Star) and converted to one-dimensional scattering by radial averaging and represented as a function of momentum transfer vector q (= $4\pi\sin\theta/\lambda$) in which θ is half the scattering angle and λ is the wavelength of the incident X-ray beam. The sample to detector distance was 0.63 m. Measurements on each sample were collected over 4 cycles of 30 min each, to ensure the stability of the lipoplexes. SAXS experiments were run at three different lipoplex compositions in the whole range of liposome.

Transmission electron microscopy (TEM) experiments were performed under liquid nitrogen temperatures (cryo-TEM). Samples of mixed liposomes in the absence and presence of DNA at different liposome compositions, and always above the

isoneutrality point of the lipoplex, were deposited on QUANTIFOIL® R 1.2/1.3 grids (http://www.quantifoil.com/) after glow discharge and rapidly vitrified in liquid nitrogen using a GATAN plunger. Grids were then observed in a JEOL JEM-1230 microscope with the temperature maintained at -180 ºC using a GATAN cryo-holder. Micrographs were recorded using a 4k x 4k TemCam-F416 camera (TVIPS). Magnifications for each camera frame varied from 10,000 to 30,000. The final sampling of each image measured in nm per pixel was calibrated using catalase crystals at each of the magnifications used. Images of individual liposomes were boxed and clipped from micrographs using the command "boxer" found in the EMAN software for image processing and the boxed images were saved as .png files. These images were visualised and filtered with "ImageJ" (Image processing and analysis in Java). A line was drawn through a desired section of each image and its profile plotted and represented using ImageJ.

Fluorescence emission spectra of ethidium bromide in the 530-700 nm region were recorded with excitation at 520 nm (the molar extinction coefficient is the same at 520 nm for free and DNA-associated EtBr) by using a Perkin Elmer LS-50B Luminescence Spectrometer.[56-59] A 10 mm stoppered rectangular silica cell was placed in a stirred cuvette holder whose temperature was kept constant at 298.15 ± 0.01 K. Probe concentration was kept constant at [EtBr] = 62.9 μM in all the cases. Two set of experiments were done: i) the emission of a EtBr/DNA solution was registered at increasing liposome concentrations by adding a EtBr/DNA/Liposome solution, thus covering a wide range of lipoplex compositions (in both solutions, DNA:EtBr molar ratio is 6:1 and [DNA] = 0.025 mg/mL; and ii) EtBr emission is measured as long as liposome concentration increases by adding an EtBr/liposome solution (blank tests). These experiments were done at different mixed liposome compositions, covering the

whole composition range. In all the cases, excitation and emission band slits were fixed at 2.5 and 5 nm, respectively, scan rate was selected at 240 nm/min.

Theoretical background. As in previous works,[16,17] the complexation of liposomes and DNA in aqueous solution has been theoretically studied by using the formalism developed by Nguyen and Shklovskii and later modified by Sennato *et al*.[50-52] This phenomenological theory describes the complexation of a long flexible polyelectrolyte of charge -*q* with oppositely charged spherical particles, such as liposomes or micelles, with charge *Q*. To this end, the authors provide the free energy of the system as a sum of the free energy related to the complexes, to the aggregates and to the remaining free polyelectrolyte in the solution. These free energies in turn depend on the fraction of polyelectrolyte in the aggregates and the number of polyelectrolytes bound to a polyelectrolyte-coated liposome complex[52] After minimizing the free energy of the system, the authors reach a set of equations that allows for the calculation of the boundaries of the region where complexes begin to condense, forming larger aggregates, and where aggregates dissolve again (re-entrant condensation). This formalism was employed in our previous works to build the complexation phase diagrams describing the condensation and re-entrant condensation behavior of different liposome-DNA complexes, as a function of the liposomes-DNA ratio.[16,17]

Herein, the theory is employed to determine the net charge of the lipoplexes studied in the present work. If we designate the number of DNA segments bound to a liposome as *N*, the charge of the lipoplexes can be defined as: $Q^* = Q - qN$. As a consequence of minimizing the free energy of the system, the values of Q^* for concentrations around the isoneutrality point are calculated by using the following equation proposed by Nguyen and Shklovskii[51] and particularized for the case of a fixed DNA concentration:

$$\frac{Q^*}{Q} = \frac{k_B TC}{qQ} \ln\left(1 + \frac{S - S_0}{S_0}\right) \qquad S_a \le S \le S_d \tag{1}$$

where S is the liposome concentration, being S_a and S_d, the boundary liposome concentrations at which the system begin to be unstable and to be re-stabilized, respectively. For values of S out of the range [S_a, S_d], the ratio Q^*/Q tends to $Z = \mp\sqrt{\frac{E_0 2C}{qQ}}$, when S tends to S_a and S_d, respectively. In these equations, $k_B T$ is the thermal energy and C is the electrical capacitance. In the case of a dispersion of spherical particles of radius a immersed in an electrolytic solution characterized by a reciprocal Debye length κ_D, the electrical capacitance can be calculated as $C = 4\pi\varepsilon_0\varepsilon a(1+\kappa_D a)$, being ε_0 and ε the vacuum and the relative permittivity, respectively. On the other hand, E_0 and S_0 are two phenomenological parameters. The former is related to the energy gained per complex by forming the aggregates (compared to a free neutral isolated liposome-DNA complex in solution) whereas S_0 is related to the isoneutrality liposome concentration (*i. e.* the liposome concentration at which the charge of the complexes is zero). If the liposome concentrations S_a and S_d are known, the phenomenological parameters can be analytically estimated from:[51]

$$S_{a,d} = S_0 \exp\left(\mp\sqrt{\frac{E_0 2qQ}{\left(k_B T\right)^2 C}}\right) \tag{2}$$

Although the Nguyen and Shklovskii complexation model describes qualitatively well experimental results, Sennato *et al*. pointed out that the theoretical description can be significantly enhanced if the Manning counterion condensation effect is taken into account. To this end, they proposed to include in the calculations renormalized charges of liposomes (Q_{ren}) and DNA molecules (q_{ren}), instead of the charges based on a full ionization of their charged groups (usually denoted as bare charges).[52] In the case of the

renormalization of the liposome charge, the authors provide a simple expression that depends on the liposome's volume fraction. In order to improve the results of Sennato *et al.* we propose a more complex renormalization calculation based on the *jellium* model that has been successfully applied in previous works for the estimation of renormalization charges of liposomes and latex particles.[60,61] The idea is to use the classical theory of colloidal stability (DLVO theory) to predict the effective interaction pair potential between two colloids but using a renormalizated charge instead of the bare charge of colloids. The whole process is detailed in the cited references and basically starts with the Poisson-Boltzmann (PB) equation for the normalized electrostatic potential in terms of the colloid bare charge. The resulting second order differential equation is solved together with the boundary conditions at the infinite distance (potential is zero) and at distance of a particle radius by applying Gauss's laws. Then the far-field solution of this equation is matched with the solution of a linearized PB equation in which the value of Q_{ren} is used instead of Q. In the case of the DNA charge, the renormalization process employed in this work will be the same as Sennato *et al.* for a general charged polyion: $q_{ren} \sim l|e|/l_B$ where l_B is the Bjerrum length $l_B = e^2/(4\pi\varepsilon_0\varepsilon k_B T)$, being e the elementary unit of charge.[52]

Results and Discussion

Liposome-DNA Interaction. It has been shown that both the composition of the mixed liposome and that of the lipoplex have a clear effect on the resulting lipoplex characteristics. For that reason, this work presents a detailed study where both compositions (liposome and lipoplex) are varied, and their effect on the resulting physicochemical properties is analyzed. Usually, liposome composition is given in terms of molar fractions, α, while either the mass ratio, L/D, or the charge ratio, CR, are

used to define the composition of the lipoplex. These latter quantities, although referred to the same magnitude, are different since *L*/*D* involves the neutral helper lipid, while CR does not. The following equations are used in this work to calculate all the abovementioned ratios:

$$\alpha = \frac{n_{L^+}}{n_{L^+} + n_{L^0}} \tag{3}$$

$$\frac{L}{D} = \frac{L^+ + L^0}{D} \tag{4}$$

$$CR = \frac{n^+}{n^-} = \frac{L^+ / M_{L^+}}{2D / \overline{M}_{bp}} \tag{5}$$

where n_{L^+}, n_{L^0} stand for the number of moles of cationic and zwitterionic lipids, respectively; n^+ and n^- are the number of moles of positive and negative charges, coming from cationic lipid and DNA, respectively; L^+ and L^0 are the masses of cationic and zwitterionic lipids (thus, $L = L^+ + L^0$, is the total mass of lipid); M_{L^+} is the molar mass of cationic lipid and $\overline{M}_{bp}$ is the average molar mass per DNA base pair.

Among all the possible *L*/*D* ratios, there is one with a special significance, the so called isoneutrality point, $(L/D)_\phi$, that is defined as the *L*/*D* ratio at which the positive charges of the liposomes neutralize the negative charges coming from the phosphate groups of DNA (i.e. the charge ratio of the lipoplexes, CR, equals 1 in eq 5). This parameter marks the lower limit of lipoplex compositions from which the net charge of the lipoplex is positive, thus becoming a potentially adequate cell transfecting agent. Three different methods have been used in this work to determine the isoneutrality point: i) through electrochemical properties, such as, electrophoretic mobility, μ_E, zeta potential, ζ, or the surface charge density enclosed by the shear plane, σ_ζ, since all of them show an inversion of sign at this particular *L*/*D* value; ii) through fluorescence

spectroscopy, by means of EtBr intercalation essays, since the maximum fluorescence intensity of the probe decreases as long as it is displaced from the hydrophobic interior of DNA helix to the bulk when the lipoplex is formed, reaching negligible values (characteristic of the probe in the bulk) at the isoneutrality of the complex; and iii) by using the theoretical model described in the previous section.

Both studies (electrochemical and spectroscopic) were run on DOEPC/DOPE-DNA lipoplexes with different DOEPC contents (α = 0.25, 0.5, 0.75 and 1) and within a *L*/*D* range that always includes the electroneutrality ratio, $(L/D)_{\phi}$. Figure 1 shows, as an example, ζ potential values as a function of *L*/*D* ratios, for the highest (α = 1) and the lowest (α = 0.25) content of DOEPC on the mixed liposome, among those studied in this work. In all the cases, ζ potentials have been obtained from electrophoretic mobility by using the well known Henry equation:

$$\zeta = \frac{3\eta}{2\varepsilon_0 \varepsilon_r f\left(\kappa_D a\right)} \mu_e \qquad (6)$$

where η is the viscosity of water (8.904×10^{-4} N m^{-2} s at 298.15 K); ε_0 and ε_r are the vacuum and relative permittivity (8.854×10^{-12} J^{-1} C^2 m^{-1} and 78.5, respectively); and $f(\kappa_D a)$ the Henry function, that depends on the reciprocal Debye length, κ_D, and the hydrodynamic particle radius, *a*. For medium-to-large particles in a medium of moderate ionic strength ($a >> \kappa_D^{-1}$), Smoluchowski limit is usually applied ($f(\kappa_D a)$ = 1.5) to estimate the Henry function.[62,63] Two characteristic sigmoid curves can be observed in Figure 1, with an inversion of sign taking place at higher $(L/D)_{\phi}$ values as long as DOEPC content decreases for a constant DNA concentration, as could be expected. The electrostatic character of the interaction that takes place between the positively charged surface of the liposome and the negatively charged DNA helix, with the release of chloride and sodium counterions from cationic lipid and DNA phosphates,

respectively, being the entropic driving force, accounts for this inversion of sign. It is also known that electrostatics plays an important role as well in various steps of the transfection process.

EtBr intercalation assays are very often used to confirm and characterize this surface electrostatic interaction, as well as to determine the isoneutrality point of the complex. EtBr is an aromatic planar cationic fluorophore whose fluorescence intensity clearly increases when it is intercalated between base pairs of double-stranded DNA.[64-68] Figure 2 shows the fluorescence of EtBr, at constant DNA concentration, at different *L*/*D* ratios for DOEPC/DOPE-DNA lipoplexes at α = 0.5, as an example (similar figures have been obtained at other lipid compositions). Also included in the figure is the EtBr fluorescence in the absence of DNA (dashed line) and also in the absence of liposomes (dotted line). A characteristic π-π^* band, centered at around 588 nm, can be observed in all the cases. It is clear from the figure that the emission of EtBr in the presence of liposomes, but in the absence of DNA, is negligible and comparable to that in the bulk, indicating that the probe does not interact with the cationic liposomes, as also found for other lipoplexes and surfoplexes.[15,16,24,32,34,35] Two complementary analysis have been done: i) one follows the emission intensity at the maximum wavelength, as a function of *L*/*D*; and ii) alternatively, the π-π^* bands have been deconvoluted, following a procedure widely explained in a previous work,[15] into overlapping gaussian curves with a non-linear least-squares multi-peaks fitting procedure, each of which being attributed to the π–π^* emission of the probe immersed within different microenvironments, characterized by its hydrophobicity, microviscosity, rigidity and/or solvation features.

Figure 3 shows the maximum emission intensity of EtBr, found at λ = 588 nm, as a function of *L*/*D*, at all the α compositions studied herein. It is remarkable that probe emission shows clear changes when DNA is present, gradually decreasing with *L/D*

from a maximum initial value, for the probe intercalated within the DNA strands, down to a constant intensity, comparable to that one found in the absence of DNA (dashed line) and even in the absence of liposomes. This behaviour confirms that DNA is compacted by the cationic surface of the liposome with an interaction that is stronger than that between EtBr and DNA, the probe being displaced by the addition of lipid from the DNA base pair hydrophobic microenvironment towards the bulk, where its quantum fluorescence yield falls down. Curves on Figure 3 allow to determine the isoneutrality points of the lipoplexes at different α values, by applying Phillip's method.[69] Figure 4 resumes these $(L/D)_{\phi}$ ratios, obtained from both the electrochemical and the spectroscopic experiments, together with those previously estimated with eq 3. It is remarkable the good concordance among all of these results. A similar behaviour was found in a previous study.[17]

Following the alternative approach, one can expect the EtBr to be immersed within two different microenvironments in the presence of DNA (the helix interior, more hydrophobic, and the buffered bulk, more polar), while in the absence of DNA it remains in only one microenvironment, the bulk. Figure 5 shows a resume of the deconvolution process into the best components (one or two gaussians) at a selection of the L/D ratios (L/D = 0, i.e. EtBr/DNA; $(L/D) < (L/D)_{\phi}$; $(L/D) > (L/D)_{\phi}$; and $L/D = \infty$, i.e. EtBr/liposomes) for DOEPC/DOPE-DNA lipoplexes at $\alpha = 0.5$ $(L/D)_{\phi,\zeta} = 5.4$), as an example. A similar behaviour has been found at all mixed liposome compositions, α. The figure confirms this transition, from two microenvironments at $L/D = 0$, to one microenvironment when EtBr is totally displaced from DNA interior towards the bulk, i.e. at $L/D > (L/D)_{\phi}$. Moreover, Figure 6, that shows a plot of the areas of the gaussians above commented as a function of the L/D ratio, is consistent with this reasoning: A_1 (blue shifted gaussian, helix interior) decreases while A_2 (red shifted gaussian, bulk)

increases with (L/D) confirming that the probe content decreases inside the helix and increases in the bulk as long as the lipoplex is formed.

Structure and Morphology of DOEPC/DOPE-DNA Lipoplexes. Lipoplex structure, size and morphology are known to be key factors on transfection efficiency.[8] In this section, DOEPC/DOPE liposomes, in the absence and in the presence of DNA, are studied by means of cryo-TEM and SAXS experiments. PALS technique also allows for the determination of the sizes of mixed liposomes; the same α compositions as those studied in the electrochemical experiments were measured. Hydrodynamic diameters of (95 ± 8), (120 ± 10), (106 ± 9), and (110 ± 10) nm were obtained at α = 0.25, 0.5, 0.75, and 1, respectively. These sizes are consistent with the sequential extrusion protocol applied in this work and also in good agreement with cryo-TEM results, as follows.

Cryo-TEM experiments were run for liposomes with α = 0.25, 0.5, 0.75, and 1, and the corresponding lipoplexes with L/D above $(L/D)_{\phi}$ in each case. Figure 7 shows a selection of cryo-TEM micrographs among those taken for the liposomes at α = 1, as an example. These images reveal that the liposomes studied herein are mostly spherical, with average diameter of around (100 ± 10) nm and a bilayer thickness of (4.2 ± 0.5) nm, both parameters averaged over the structures found in all the micrographs (not only over those shown herein). It is remarkable that, in contrast with what was found in previous studies[15-17,70] where liposomes were mostly unilamellar, an appreciable percentage of multilamelar structures can be observed in the present case, together with a remarkable increase on the flexibility of the membranes that justify the presence of looped and twisted and invaginated structures This feature is consistent with the structure of DOEPC molecule that, as in the case of DOPE (see Scheme 1), has a single olefinic unsaturation on the *cis* configuration at the 9 position in the two 18C hydrocarbon chains. In fact, it has been demonstrated that the presence of this double

bond is the responsible of the low T_m of these lipids (T_m for DOPE is around -16 ºC), and, accordingly, of their abilities as fusogenic lipids. It is then expected that DOEPC/DOPE liposomes would show improved characteristics as cell transfectors.

Cryo-TEM experiments were also run on positively charged lipoplex samples, i.e. at (L/D) ratios above $(L/D)_\phi$. Figure 8 shows a gallery of selected micrographs of DOEPC/DOPE-DNA lipoplexes at the different α compositions studied in this work. Compared with the micrographs of Figure 7, it can be clearly seen that lipoplexes are more condensed than liposomes, with an accumulation of density on the surface. It is remarkable that the neat characteristic contrast between the line representing the lipidic bilayer and the interior of the liposomes has been lost in most cases. These features confirm that DNA is compacted at the surface of liposomes by means of a strong electrostatic interaction, as corroborated by zeta potential and fluorescence results. As can be seen in the figure, multilamellar structures are found as well in the case of lipoplexes. However, note that these structures are different that those found for multilamellar liposomes of Figure 8. Some of those micrographs, where multilamellar onion-type lipoplexes are observed, were chosen to analyze the presence of possible patterns of periodicity that would confirm the regular arrangement of the multilamellae. These selected micrographs were analyzed with the image processing protocol explained in the Experimental Section. Thus, a solid line was drawn perpendicular to the membranes to plot the variations in density, which appear as different grey levels in the TEM images. Figure 9 shows a plot of grey levels vs. distance along the line drawn in panel A as represented by ImageJ (Image processing and analysis in Java), for α = 0.5, 0.75 and 1, as an example. The maximum and minimum levels of density revealed a clear pattern and the average distance between peaks, measured in pixels, was calculated and transformed in nm using the nm/pixel scale for each image. As can be

seen in Figure 9, a complex profile with several peaks and a wider dimension, indicate the presence of several layers. Averaged interlamellar spacing of (6.7 ± 0.4 nm), (6.9 ± 0.3 nm), and (7.2 ± 0.3 nm), respectively, confirms the compaction of DNA helixes on a multilamellar sanwhiched structure (~4.4 nm/bilayer + ~2.5 nm/DNA helix), although a more precise and detailed analysis will be presented in the following section where SAXS experiments are reported.

The structures of the cationic lipoplexes were also investigated by SAXS. The experiments were carried on covering the whole composition range of the lipid composition, α, at three charge ratios, CR (= 3, 5 and 7). Figure 10a-c shows all SAXS diffractograms, the intensity being plotted vs q factor. Bragg peaks show that, for $\alpha \geq 0.4$, lipoplexes form a lamellar structure, L_α, according to Scheme 2 (three related sharp peaks have been found for each diffractogram) with an interlayer distance, d, related to the q factor of first peak ($d = 2\pi/q_{100}$). Thus, lipoplexes may be represented as alternating layers of mixed lipids and DNA helixes, where d (= $d_m + d_w$) is the sum of the thicknesses of the lipid bilayer, d_m, and the DNA aqueous layer, d_w. Accordingly, the Bragg peak on each diffractogram not corresponding to the lamellar structure arise from the DNA-DNA correlation, and, from q_{DNA}factor, DNA strands separation in the monolayer, d_{DNA}, (= $2\pi/q_{DNA}$) can be calculated (see Scheme 2). In those cases where peaks are difficult to see, a protocol based on the second derivative of the intensity was applied in the region where the peak is expected. Plots of the periodic distance of the lamellar structure, d, vs α, at the three charge ratios, reported in Figure 11, indicate that d remains constant within an average value of (6.6 ± 0.2) nm. This feature is due to the fact that DOEPC and DOPE lipids have a hydrophobic region of identical length, (Scheme 1) and the thickness of the mixed lipid bilayer, d_m, must not change with the lipid composition. If a value of $d_m \approx 4.2$ nm is assumed, a thickness of the DNA

monolayer, d_w (= 2.4 ± 0.2) nm, independent of α, and CR, is obtained, completely consistent with the presence of a monolayer of the hydrated DNA helixes. The results for d and d_m for the lamellar structure are consistent with those ones previously obtained from cryo-TEM experiments. Furthermore, Figure 12 shows how the separation between the DNA helixes, d_{DNA}, slightly decreases with α at the three charge ratios, since one would expect that, at constant CR, d_{DNA} should decreases as increases the cationic lipid content in the lipoplex, α, a behavior already reported in the literature for other lipoplexes.[71] In addition, SAXS results are in good agreement with reported cryo-TEM micrographs, and confirm the presence of multilamellar structures for DOEPC/DOPE-DNA lipoplexes above the isoneutrality.[70] Similar conclusions were also extracted for other lipoplexes reported previously.[15,16]

Nevertheless, the Bragg peaks observed on SAXS diffractogram at α = 0.2 of Figure 10a-c, index nicely on a 2*D* hexagonal lattice, H_{II}, similar to that one shown on Scheme 2. The spacing of the cell unit can be also directly related to the q factor ($d = d_{DNA} = 4\pi/(3^{(1/2)}q_{10})$. In this lattice, a monolayer of mixed lipids with the zwitterionic DOPE as the main component, surrounds the DNA helixes, the structure of the DNA-mixed lipids resembling inverted cylindrical micelles. The constant value of (7.8 ± 0.2) nm obtained for d (= d_{DNA}), at the three charge ratios (see Figure 11), indicates that the periodicity of the lipid structure is higher in the hexagonal packing than in the lamellar one. Moreover, since $d = d_{DNA}$ for H_{II} phase, it can be concluded as well that DNA helixes are more separated that in L_α phase, where d_{DNA} values fall around 5 nm (see Figure 12). In any case, and taking into account the lipid chain lengths, the diameter inside the inverted micelle cylinder (equivalent to d_w in the lamellar structure) is (3.6 ± 0.2) nm, enough to host the hydrated DNA helixes.

It has been confirmed[5,72,73] that, in the early stage of the transfection, the interaction between positive lipoplexes and anionic membranes is strongly dependent on the lipoplex structure. In fact, lamellar lipoplexes captured by endosomal vesicles remain stable being the DNA release relatively low, while hexagonal lipoplexes rapidly fused with the anionic endosomal vesicle, provoking a loosing of the lipoplex condensed structure, and accordingly, DNA is easier released to the cytoplasm,[72] with proved better efficiency in transfection than lamellar ones.[73,74] Accordingly, it could be concluded that the DOEPC/DOPE-DNA lipoplex studied in this work, is potentially an adequate gene vector when the cationic lipid content is moderate-to-low, since above the isoneutrality an inverted hexagonal phase has been found in such cases irrespectively of the positive charge ratio of the lipoplex. Nevertherless, cytotoxicity and transfection assays would be necessary to confirm it.

Theoretical Calculations. Figure 13 shows the values for Q_{ren} as a function of Q, calculated by using the renormalization process described in the theoretical background section of this work and the experimental conditions of the lipoplexes herein studied. As can be seen in the figure, results point out how Q increases linearly with Q_{ren} for low values of the bare charge (note that Q matches Q_{ren} only at very low Q values). In contrast, Q reaches a saturation regime for high values of Q. Under this situation, an increase of the bare charge of liposomes does not involve a proportional variation of their effective charge.

The effective surface charge has been evaluated from the measurement of electrochemical parameters of the lipid vesicles by Bordi *et al.*[75] In particular, these authors compared the effective charge with the structural one, derived from the full ionization of the surface charged groups. According with their results, a strong charge renormalization must be invoked to account for the electrochemical properties of

liposomes. Following this approach, renormalization data from Figure 13 will be used in this work to analyze the electrophoretic mobility measurements of our systems together with the complexation model of Sklovskii *et al*. According to this theory, the isoneutrality point can be theoretically predicted by means of eq 2 and using the electrokinetic experiments. In particular, the values of S_a and S_d, obtained from electrophoresis measurements, are used as inputs in eq 2 to calculate the phenomenological parameters S_0 and E_0. Table 3 resumes the results obtained for the lipoplexes studied in this work, together with those obtained for other lipoplexes previously studied by our group.[17]

On the one hand the values estimated for E_0 are much higher than those obtained in previous cases for similar systems.[16,17] This is principally due to definition of the electric capacitance used therein, that did not include the effect of the ionic strength of the media. As a consequence, the salt-free values of C used to solve eq 2 in our previous works were considerably low and less realistic than that proposed in the present work (see theoretical section). On the other hand, if S_0 is directly identified with the isoneutrality liposome concentration (as the model suggests), the agreement with the experiments is quite good, as can be observed in Figure 4, where S_0 values, expressed in terms of $(L/D)_\phi$, are also included. Moreover, the theoretical values of S_0 can be also used to estimate the charge of lipoplexes for L/D ratios around the isoneutrality point. To this end, eq 1 is solved for each system. However, instead of the bare charges of liposomes and DNA, the calculations have been done using the renormalization values according to the *jellium* model described in the theoretical background section (see Figure 13). Accordingly, by using the data shown in Table 3 and eq 1, Q^*/Q_{ren} can be plotted as a function of the liposome concentration (Figure 14). This figure clearly shows how the values S_0 are always within the experimental range [S_a, S_d] and

correspond to the liposome concentration at which $Q^*/Q_{ren} = 0$. In general, the results shown in the Figure 14 exhibit the behaviour predicted theoretically; in the cited range, Q^*/Q_{ren} varies according with eq 1 and it tends to $Z = \mp\sqrt{\frac{E_0 2C}{q_{ren}Q_{ren}}}$, when S tends to S_a and S_d, respectively. It is also remarkable that the trend shown by experimental electrophoretic measurements in Figure 4 (for DOEPC/DOPE-DNA lipoplexes at α = 0.25 and 1) is in very good agreement with that one presented by theoretical calculations in Figure 14.

Regarding the maximum magnitude of Q^*, $|Q^*|_{max} = |Q_{ren}Z|$, it generally increases with the charge of the liposomes (see Table 3). This feature confirms the fact that the electrostatic interaction is the driving force in the formation of the complexes. However, the increase tends to be slower as the liposome charge is higher. This is a direct consequence of the renormalization process in which Q_{ren} tends to reach a saturation value as Q increases (see Figure 13). In other words, although the charge of the liposomes favors the formation of liposome-DNA complexes and the increase of $|Q^*|_{max}$, the model predicts that the number of DNA segments bound to each liposome, will reach a saturation value in such way that it will not depend on the liposome charge. For instance, comparing the values $|Q^*|_{max}$ corresponding to DOEPC/DOPE-DNA at α = 0.5 and 1, they are very similar despite the fact that the bare charge of the latter is almost twice the bare charge of the former. This feature have also observed in previous works[17] and implies that once the surface charge of liposomes is large enough, this is not the only parameter that favors the complexation of DNA with liposomes. In other words, zwitterionic helper lipids play also an important role in the formation of lipoplexes. Apart from that, the results also show the effect of the cationic lipid molar fraction α on the lipoplex charge, in a very good agreement with the experimental

findings, i.e. the isoneutrality is shifted towards lower experimental *L*/*D* values (see Figures 1 or 4) and/or theoretical *S* values (see Figure 14), as long as α increases.

Conclusions

A wide physicochemical study, consisting of both experimental (electrophoretic mobility, fluorescence spectroscopy, cryo-TEM and SAXS studies) and theoretical approaches, has evidenced that CT-DNA is properly condensed and compacted by DOEPC/DOPE cationic liposomes via a strong surface electrostatic interaction. DOEPC/DOPE liposomes are mainly spherical with a diameter of around (100 ± 10) nm and a lipidic bilayer of around (4.5 ± 0.5) nm thick showing an appreciable percentage of multilamellar structures. Furthermore, cryo-TEM micrographs reveal that DOEPC/DOPE mixed liposomes may present a variety of looped, twisted and invaginated structures that is consistent with the fact that this mixed lipidic membrane shows a relative high elasticity and, accordingly, increases the fusogenic capacity in the lipoplex. The periodicity of around 7 nm in the multilamellar structures on lipoplexes has been determined by digitizing and image processing techniques, indicating that DNA helixes are effectively sandwiched and aligned between cationic lipid bilayers. The isoneutrality of the lipoplex thus formed, determined by zeta potential, EtBr intercalation essays, and theoretical calculations decreases with the content on cationic lipid on the mixed liposome. This molar fraction has also a marked effect on lipoplex structures, which goes from inverted hexagonal phase, H_{II}, at low cationic lipid contents ($\alpha \approx 0.2$) to lamellar phase, L_α, at $\alpha \geq 0.4$. The experimental results are in very good agreement with the theoretical model used in this work, reinforcing that a charge renormalization must be invoked to account for the electrochemical properties of liposomes and lipoplexes.

Acknowledgment. The authors thank MICINN of Spain (Projects No. CTQ2009-10002BQU, SAF2008-00451, MAT2008-03232, MAT2009-13155-C04-04 and UCMA05-33-010), the CSIC (Project No. PIE200750-I021), the Comunidad Autónoma of Madrid (Projects No. S-SAL-0249-2006, and CAM S-BIO-0214-2006), the Junta de Andalucía (Projects No. P07-FQM-02517 and P09-FQM-4698), the "Red Temática de Investigación Cooperativa en Cáncer (RTICC)" from the "Instituto de Salud Carlos III" (RD06/0020/1001), the Human Frontiers Science Program (RGP39/2008), and the Universidad Complutense of Madrid (Project No. GR58-08). Authors also thank C. Aicart for carrying on gel agarose electrophoresis experiments at the Biochemistry and Molecular Biology Department of the UCM of Spain.

References and Notes

(1) Felgner, J. H.; Gadek, T. R.; Holm, M.; Roman, R.; Chan, H. W.; Wenz, M.; Northrop, J. P.; Ringold, G. M.; Danielsen, M., *Proc. Natl. Acad. Sci. U.S.A.* **1987**, *84*, 7413-7417.

(2) Felgner, P. L.; Heller, M. J.; Lehn, J. M.; Behr, J.-P.; Szoka, F. C., *Artificial Self-Assembling Systems for Gene Delivery*. American Chemical Society: Washington, DC, 1996.

(3) Mahato, R. I.; Kim, S. W., *Pharmaceutical Perspectives of Nucleic Acid-Base Therapeutics*. Taylor and Francis: London, 2002.

(4) Lasic, D. D., *Liposomes in Gene Delivery*. CRC Press: Boca Raton, FL, 1997.

(5) Ewert, K.; Slack, N. L.; Ahmad, A.; Evans, H. M.; Lin, A. J.; Samuel, C. E.; Safinya, C. R., *Curr. Med. Chem.* **2004**, *11*, 133-149.

(6) Lonez, C.; Vandenbranden, M.; Ruysschaert, J. M., *Progress in Lipid Research* **2008**, *47*, 340-347.

(7) Ma, B. C.; Zhang, S. B.; Jiang, H. M.; Zhao, B. D.; Lv, H. T., *J. Controlled Release* **2007**, *123*, 184-194.

(8) Safinya, C. R.; Ewert, K.; Ahmad, A.; Evans, H. M.; Raviv, U.; Needleman, D. J.; Lin, A. J.; Slack, N. L.; George, C.; Samuel, C. E., *Philos. Trans. R. Soc., A* **2006**, *364*, 2573-2596.

(9) Bajaj, A.; Kondaiah, P.; Bhattacharya, S., *Bioconjugate Chem.* **2007**, *18*, 1537-1546.

(10) Bajaj, A.; Kondaiah, P.; Bhattacharya, S., *Biomacromolecules* **2008**, *9*, 991-999.

(11) Dias, R. S.; Lindman, B., *DNA Interaction with Polymers and Surfactants*. Wiley & Sons: Hoboken, 2008.

(12) Caracciolo, G.; Caminiti, R., *Chem. Phys. Lett.* **2005**, *411*, 327-332.

(13) Caracciolo, G.; Pozzi, D.; Amenitsch, H.; Caminiti, R., *Langmuir* **2005**, *21*, 11582-11587.

(14) Ciani, L.; Casini, A.; Gabbiani, C.; Ristori, S.; Messori, L.; Martini, G., *Biophys. Chem.* **2007**, *127*, 213-220.

(15) Rodriguez-Pulido, A.; Aicart, E.; Llorca, O.; Junquera, E., *J. Phys. Chem. B* **2008**, *112*, 2187-2197.

(16) Rodriguez-Pulido, A.; Martin-Molina, A.; Rodriguez-Beas, C.; Llorca, O.; Aicart, E.; Junquera, E., *J. Phys. Chem. B* **2009**, *113*, 15648-15661.

(17) Munoz-Ubeda, M.; Rodriguez-Pulido, A.; Nogales, A.; Martin-Molina, A.; Aicart, E.; Junquera, E., *Biomacromolecules* **2010**, *11*, 3332-3340.

(18) Lin, A. J.; Slack, N. L.; Ahmad, A.; George, C. X.; Samuel, C. E.; Safinya, C. R., *Biophys. J.* **2003**, *84*, 3307-3316.

(19) Lasic, D. D.; H., S.; Stuart, M. A. C.; R., P.; Frederik, P., *J. Am. Chem. Soc.* **1997**, *119*, 832-833.

(20) Barreleiro, P. C. A.; Olofsson, G.; Brown, W.; Edwards, K.; Bonassi, N. M.; Feitosa, E., *Langmuir* **2002**, *18*, 1024-1029.

(21) Feitosa, E.; Alves, F. R.; Niemiec, A.; Oliveira, M.; Castanheira, E. M. S.; Baptista, A. L. F., *Langmuir* **2006**, *22*, 3579-3585.

(22) Salvati, A.; Ciani, L.; Ristori, S.; Martini, G.; Masi, A.; Arcangeli, A., *Biophys. Chem.* **2006**, *121*, 21-29.

(23) Gustafsson, J.; Arvidson, G.; Karlsson, G.; Almgren, M., *Biochim. Biophys. Acta* **1995**, *1235*, 305-312.

(24) Xu, Y. H.; Hui, S. W.; Frederik, P.; Szoka, F. C., *Biophys. J.* **1999**, *77*, 341-353.

(25) Hirsch-Lerner, D.; Zhang, M.; Eliyahu, H.; Ferrari, M. E.; Wheeler, C. J.; Barenholz, Y., *Biochim. Biophys. Acta* **2005**, *1714*, 71-84.

(26) Zuidam, N. J.; Barenholz, Y., *Biochim. Biophys. Acta* **1998**, *1368*, 115-128.

(27) Janoff, A. S., *Liposomes: Rational Design*. Marcel Dekker: New York, 1999.

(28) Rosoff, M., *Vesicles*. Marcel Dekker: New York, 1996.

(29) Rädler, J. O.; Koltover, I.; Jamieson, A.; Salditt, T.; Safinya, C. R., *Langmuir* **1998**, *14*, 4272-4283.

(30) Birchall, J. C.; Kellaway, I. W.; Mills, S. N., *Int. J. Pharm.* **1999**, *183*, 195-207.

(31) Lobo, B. C.; Rogers, S. A.; Choosakoonkriang, S.; Smith, J. G.; Koe, G. S.; Middaugh, C. R., *J. Pharm. Sci.* **2001**, *91*, 454-466.

(32) Eastman, S. J.; Siegel, C.; Tousignant, J.; Smith, A. E.; Cheng, S. H.; Scheule, R. K., *Biochim. Biophys. Acta* **1997**, *1325*, 41-62.

(33) Lakowicz, J. R., *Principles of Fluorescence Spectroscopy*. Kluwer Acad./Plenum: New York, 1999.

(34) MacDonald, R. C.; Ashley, G. W.; Shida, M. M.; Rakhmanova, V. A.; Tarahovsky, Y. S.; Pantazatos, D. P.; Kennedy, M. T.; Pozharski, E. V.; Baker, K. A.; Jones, R. D.; Rosenzweig, H. S.; Choi, K. L.; Qiu, R.; McIntosh, T. J., *Biophys. J.* **1999**, *77*, 2612-2629.

(35) Tarahovsky, Y. S.; Koynova, R.; MacDonald, R. C., *Biophys. J.* **2004**, *87*, 1054-1064.

(36) Bhattacharya, S.; Mandal, S. S., *Biochemistry* **1998**, *37*, 7764-7777.

(37) Geall, A. J.; Eaton, M. A. W.; Baker, T.; Catterall, C.; Blagbrough, I. S., *FEBS Lett.* **1999**, *459*, 337-342.

(38) Borenstain, V.; Barenholz, Y., *Chem. Phys. Lipids* **1993**, *64*, 117-127.

(39) Hirsch-Lerner, D.; Barenholz, Y., *Biochim. Biophys. Acta* **1998**, *1370*, 17-30.

(40) Lentz, B. R.; Moore, B. M.; Barrow, D. A., *Biophys. J.* **1979**, *25*, 489-494.

(41) Regelin, A. E.; Fankhaenel, S.; Gurtesch, L.; Prinz, C.; von Kiedrowski, G.; Massing, U., *Biochim. Biophys. Acta* **2000**, *1464*, 151-164.

(42) Ryhänen, S. J.; Säily, M. J.; Paukku, T.; Borocci, S.; Mancini, G.; Holopainen, J. M.; Kinnunen, P. K., *Biophys. J.* **2003**, *84*, 578-587.

(43) Alfredsson, V., *Curr. Opin. Colloid Interface Sci.* **2005**, *10*, 269-273.

(44) Dias, R. S.; Lindman, B.; Miguel, M. G., *J. Phys. Chem. B* **2002**, *106*, 12600-12607.

(45) Huebner, S.; Battersby, B. J.; Grimm, R.; Cevc, G., *Biophys. J.* **1999**, *76*, 3158-3166.

(46) Mel'nikova, Y. S.; Mel'nikov, S. M.; Lofroth, J. E., *Biophys. Chem.* **1999**, *81*, 125-141.

(47) Scarzello, M.; Chupin, V.; Wagenaar, A.; Stuart, M. C. A.; Engberts, J. B. F. N.; Hulst, R., *Biophys. J.* **2005**, *88*, 2104-2113.

(48) Silvander, M.; Edwards, K., *Anal. Biochem.* **1996**, *242*, 40-44.

(49) Smisterova, J.; Wagenaar, A.; Stuart, M. C. A.; Polushkin, E.; Brinke, G.; Hulst, R.; Engberts, J. B. F. N.; Hoekstra, D., *J. Biol. Chem.* **2001**, *276*, 47615-47622.

(50) Nguyen, T. T.; Shklovskii, B. I., *J. Chem. Phys.* **2001**, *114*, 5905-5916.

(51) Nguyen, T. T.; Shklovskii, B. I., *J. Chem. Phys.* **2001**, *115*, 7298-7308.

(52) Sennato, S.; Bordi, F.; Cametti, C., *J. Chem. Phys.* **2004**, *121*, 4936-4940.

(53) Barreleiro, P. C. A.; Lindman, B., *J. Phys. Chem. B* **2003**, *107*, 6208-6213.

(54) Mel'nikov, S. M.; Lindman, B., *Langmuir* **1999**, *15*, 1923-1928.

(55) Gonçalves, E.; Debs, R. J.; Heath, T. D., *Biophys. J.* **2004**, *86*, 1554-1563.

(56) Junquera, E.; Peña, L.; Aicart, E., *Langmuir* **1997**, *13*, 219-224.

(57) Junquera, E.; del Burgo, P.; Boskovic, J.; Aicart, E., *Langmuir* **2005**, *21*, 7143-7152.

(58) Junquera, E.; Aicart, E., *Int. J. Pharm.* **1999**, *176*, 169-178.

(59) Merino, C.; Junquera, E.; Jimenez-Barbero, J.; Aicart, E., *Langmuir* **2000**, *16*, 1557-1565.

(60) Haro-Perez, C.; Quesada-Fernandez, M.; Callejas-Fernandez, J.; Sabate, E.; Estelrich, J.; Hidalgo-Alvarez, R., *Colloids Surf. A* **2005**, *270*, 352.

(61) Haro-Perez, C.; Quesada-Perez, M.; Callejas-Fernandez, J.; Shurtenverger, P.; Hidalgo-Alvarez, R., *J. Phys.: Condens. Matter* **2006**, *18*, L363-L369.

(62) Delgado, A. V., *Interfacial Electrokinetics and Electrophoresis*. Marcel Dekker: New York, 2002; Vol. 106.

(63) Ohshima, H.; Furusawa, K., *Electrical Phenomena at Interfaces. Fundamentals, Measurements, and Applications*. Marcel Dekker: New York, 1998.

(64) Congiu, A.; Pozzi, D.; Esposito, C.; Castellano, C.; Mossa, G., *Colloids Surf., B* **2004**, *36*, 43-48.

(65) Esposito, C.; Generosi, J.; Mossa, G.; Masotti, A.; Castellano, A. C., *Colloids Surf., B* **2006**, *53*, 187-192.

(66) Farhood, H.; Serbina, N.; Huang, L., *Biochim. Biophys. Acta* **1995**, *1235*, 289-295.

(67) Tarahovsky, Y. S.; Rakhmanova, V. A.; Epand, R. M.; MacDonald, R. C., *Biophys. J.* **2002**, *82*, 264-273.

(68) Caplen, N. J.; Alton, E. W.; Middleton, P. G.; Dorin, J. R.; Stevenson, B. J.; Gao, X.; Durham, S. R.; Jeffrey, P. K.; Hodson, M. E., *Nat. Med.* **1995**, *1*, 39-46.

(69) Phillips, J. N., *Trans. Faraday Soc.* **1955**, *51*, 561-569.

(70) Rodriguez-Pulido, A.; Ortega, F.; Llorca, O.; Aicart, E.; Junquera, E., *J. Phys. Chem. B* **2008**, *112*, 12555-12565.

(71) Koltover, I.; Salditt, T.; Safinya, C. R., *Biophys. J.* **1999**, *77*, 915-924.

(72) Koltover, I.; Salditt, T.; Rädler, J. O.; Safinya, C. R., *Science* **1998**, *281*, 78-81.

(73) Pozzi, D.; Caracciolo, G.; Caminiti, R.; De Sanctis, S. C.; Amenitsch, H.; Marchini, C.; Montani, M.; Amici, A., *Appl. Mat. Interfaces* **2009**, *1*, 2237-2249.

(74) Bouxsein, N. F.; McAllister, C. S.; Ewert, K. K.; Samuel, C. E.; Safinya, C. R., *Biochemistry* **2007**, *46*, 4785-4792.

(75) Bordi, F.; Cametti, C.; Sennato, S.; Paoli, B.; Marianecci, C., *J. Phys. Chem. B* **2006**, *110*, 4808-4814.

Figure Legend

Figure 1. Plot of zeta potential, ζ, as a function of lipoplex composition, *L*/*D*, for lipoplexes with α = 0.25 and 1, in aqueous buffered medium at 298.15 K. Solid line: sigmoidal fit of experimental values. Errors are estimated to be around 3%. DNA concentration was kept constant at 0.0491 mg/mL and the total lipid concentration was varied, depending of the lipid composition, to cover a wide *L*/*D* ratio range.

Figure 2. Emission fluorescence spectra of EtBr in the presence of DOEPC/DOPE-DNA lipoplexes at α = 0.5 and different *L/D* ratios: 0, *L/D* = 0; 1, *L*/*D* = 1.0; 2, *L*/*D* = 2.0; 3, *L*/*D* = 3.0; 4, *L*/*D* = 4.0; 5, *L*/*D* = 5.0; 6, *L*/*D* = 6.0; 7, *L*/*D* = 7.0; dotted line shows the emission fluorescence spectra of EtBr in the absence of liposomes and lipoplexes; and dashed line shows the emission fluorescence spectra of EtBr only in presence of liposomes (*L*/*D* = ∞). Medium: aqueous PBS 160 mM, pH = 7.5. DOEPC:DOPE ratio is 1:1; DNA:EtBr ratio is 6:1; [DNA] = 0.025 mg/mL.

Figure 3. Emission fluorescence intensity of EtBr at 588 nm in the presence of DOEPC/DOPE-DNA lipoplexes as a function of *L*/*D* ratio at different mixed liposome compositions, α = 0.25, 0.5, 0.75 and 1. Medium: aqueous PBS 160 mM, pH = 7.5. DNA:EtBr ratio is 6:1; [DNA] = 0.025 mg/mL. Dashed line shows an example of the emission fluorescence spectra of EtBr only in presence of liposomes.

Figure 4. Plot of isoneutrality *L*/*D* ratios, $(L/D)_{\phi}$, as a function of mixed liposome composition in terms of molar fractions, α. The figure shows the results obtained from electrophoretic measurements and EtBr intercalation assays, together with those estimated with eq 3 and those calculated with the theoretical model.

Figure 5. Emission fluorescence spectra of EtBr in the presence of DOEPC/DOPE-DNA lipoplexes at α = 0.5 and at a selection of *L*/*D* ratios, together with their

deconvolutions into 1 or 2 gaussian components: L/D = 0, only DNA; L/D = 2.0, below $(L/D)_\phi$; L/D = 6, above $(L/D)_\phi$; and $L/D = \infty$, only DOEPC/DOPE liposomes. Black line: experimental spectra. Blue lines: gaussian components. Red line in 2 gaussian cases: total sum of gaussian components. Medium: aqueous PBS 160 mM, pH = 7.5.

Figure 6. Plot of the areas (in terms of % of the total area) of gaussian bands as a function of L/D ratios for DOEPC/DOPE-DNA (solid symbols, A_1, and empty symbols, A_2) at different mixed liposome compositions, α = 0.25, 0.5, 0.75 and 1.

Figure 7. Details extracted from the original cryo-TEM micrographs of liposomes in the absence of DNA, i.e. at $L/D = \infty$ and α = 1. Scale bar: 100 nm.

Figure 8. Details extracted from the original cryo-TEM micrographs of DOEPC/DOPE-DNA lipoplexes at $L/D > (L/D)_\phi$: (a) α = 0.25; (b) α = 0.5; (c) α = 0.75 and (d) α = 1. Scale bar: 100 nm in figures (a) and (c); 200 nm in figures (b) and (d)

Figure 9. (A) A selected view of DOEPC/DOPE-DNA multilamellar lipoplexes as observed in the electron microscopy at different mixed liposome compositions, α. A solid black line was drawn perpendicular to the membranes to plot the variations in density, which appear as different grey levels in the TEM images. (B) Plot of grey levels along the line drawn in panel A as represented by ImageJ (Image processing and analysis in Java). The average distance between peaks, measured in pixels, was calculated and transformed in nm using the nm/pixel scale for each image: at α = 1, 12.67 pixels (5.68 nm/pixel) = 7.2 nm; at α = 0.75, 18.5 pixels (0.375 nm/pixel) = 6.9 nm; and at α = 0.5, 6.25 pixels (1.075 nm/pixel) = 6.7 nm.

Figure 10. Diffractograms of DOEPC/DOPE-DNA lipoplexes at different mixed lipid composition, α, and a charge ratio CR = 3 (a), 5 (b) and 7 (c). DNA concentration was varied from 0.6 to 2.0 mg/mL for CR = 3, from 0.38 to 1.48 mg/mL for CR = 5 and from 0.26 to 1.09 mg/mL for CR = 7. Total lipid concentration was varied from from 15.5 to 20.3 mg/mL for CR = 3, from 18.4 to 21.3 mg/mL for CR = 5 and from 19.9 to 21.8 mg/mL for CR = 7.

Figure 11. Plots of the periodic distance of the lamellar structure, d, as a function of α, at charge ratios, CR, of 3 (squares), 5 (circles) and 7 (triangles). Open symbols: L_α structure, $\alpha \geq 0.4$; solid symbols: H_{II} structure, $\alpha = 0.2$.

Figure 12. Plots of the distance between DNA helixes, d_{DNA}, as a function of α, at charge ratios, CR, of 3 (squares), 5 (circles) and 7 (triangles). Open symbols: L_α structure, $\alpha \geq 0.4$; solid symbols: H_{II} structure, $\alpha = 0.2$.

Figure 13. Renormalized charges provided by the jellium model (particle radius: 49.5 nm, volume fraction: 0.02, ionic strength: 160 mM and temperature: 298 K), as a function of the bare charge of liposomes.

Figure 14. Theoretical charge of lipoplexes calculated from eq 1 and normalized by the renormalized charge, as a function of the liposome concentration.

(a)

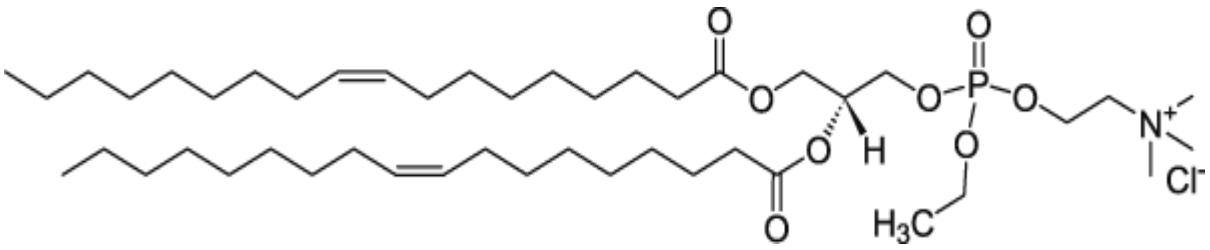

(b)

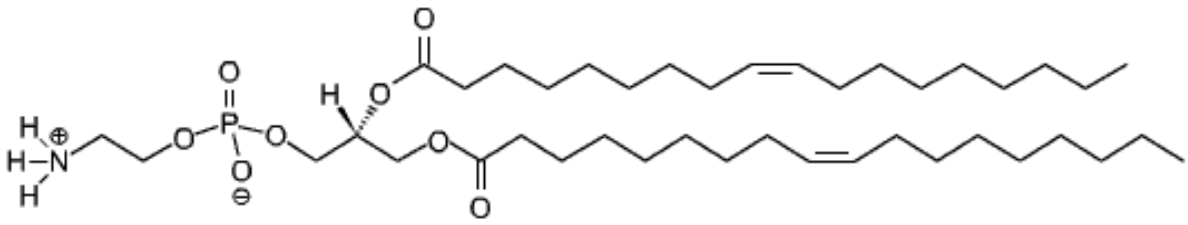

SCHEME 1. (a) Cationic lipid molecule, DOEPC; and (b) Zwiterionic lipid molecule, DOPE.

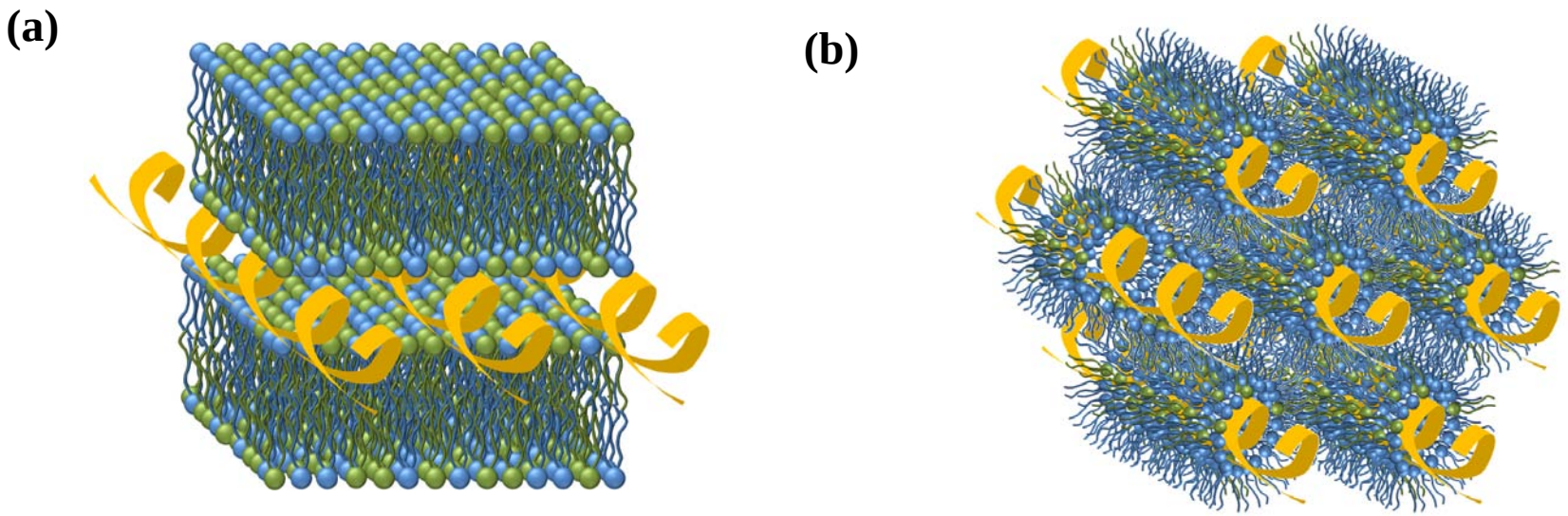

SCHEME 2. (a) Lamellar structure, L_{α}, and; (b) Inverted hexagonal structure, H_{II}.

Table 1. Values of electrophoretic mobility, μ_e, zeta potential, ζ, and surface density charge (at the shear plane), σ_ζ, at a series of mixed liposome composition, α, and, within each a composition, at different values of *L*/*D* mass ratios, for DOEPC/DOPE/CT-DNA lipoplexes. DNA concentration was kept constant at 0.049 ± 0.001 mg/mL.

L/*D*	$\mu_E \cdot 10^8$ / $m^2V^{-1}s^{-1}$	ζ / mV	$10^3\,\sigma_\zeta$ / Cm^{-2}
α = 0.25			
3.0	- 4.12	- 53.4	-18.6
5.0	- 4.18	- 54.2	-19.0
7.0	- 4.16	- 53.9	-18.8
11.0	2.03	26.3	8.1
13.0	2.32	29.7	9.6
15.0	2.99	35.5	11.3
∞[a]	2.07	26.8	8.2
α = 0.50			
L/*D*	$\mu_E \cdot 10^8$ / $m^2V^{-1}s^{-1}$	ζ / mV	$10^3\,\sigma_\zeta$ / Cm^{-2}
1.5	- 3.98	- 51.6	-17.8
3.0	- 3.90	- 50.6	-17.4
4.0	- 3.85	- 49.9	-17.0
6.0	1.52	19.7	5.9
7.0	2.36	30.6	9.5
9.0	3.22	41.7	13.6
∞	2.91	37.7	12.1
α = 0.75			
L/*D*	$\mu_E \cdot 10^8$ / $m^2V^{-1}s^{-1}$	ζ / mV	$10^3\,\sigma_\zeta$ / Cm^{-2}
1.0	- 4.44	- 57.6	-20.6
2.0	- 4.26	- 55.3	-19.6
3.0	- 4.37	- 56.6	-20.1
5.0	3.62	46.9	15.7
7.0	3.79	49.1	16.7
9.0	3.91	50.7	17.4
∞	3.06	39.7	12.9
α = 1			
L/*D*	$\mu_E \cdot 10^8$ / $m^2V^{-1}s^{-1}$	ζ / mV	$10^3\,\sigma_\zeta$ / Cm^{-2}
0.8	- 4.47	- 58.0	-21.6
1.3	- 4.65	- 60.3	-22.0
2.0	- 4.20	- 54.5	-19.1
3.0	-0.54	-7.00	2.06
5.0	4.02	52.1	18.0
8.0	4.09	53.0	18.6
∞	4.33	56.1	20.1

[a]Mixed liposomes in the absence of DNA [b]Errors are estimated to be around 3% in electrophoretic mobility and zeta potential and around 6% in surface density charge.

Table 2. Values of interlayer distance, *d*, and DNA strands separation within the monolayer, d_{DNA}, at different *L*/*D* ratios and mixed liposome compositions, α, for DOEPC/DOPE-DNA lipoplexes at CR = 3, 5 and 7.

	CR = 3.0			CR = 5.0			CR = 7.0		
α	*d*/ nm	d_{DNA}/nm	*L*/*D*	*d*/ nm	d_{DNA}/nm	*L*/*D*	*d*/ nm	d_{DNA}/nm	*L*/*D*
1[a]	6.4	3.8	7.9	6.4	4.4	12	6.4	4.0	18
0.8[a]	–	–	9.6	6.4	4.5	15	6.5	4.1	22
0.6[a]	6.9	4.5	12	6.5	4.7	20	6.5	4.5	29
0.5[a]	6.4	3.8	15	6.5	4.5	23	6.7	4.6	34
0.4[a]	–	–	18	6.7	5.1	29	6.7	5.0	42
0.2[b]	7.7		35	7.8		56	7.8		82

[a] Lamellar L_α structure
[b] Hexagonal H_{II} structure ($d = d_{DNA}$)

Table 3. Renormalized charges provided by the jellium model (Q_{ren}), phenomenological parameters of the eq 2 (S_0 and E_0) and maximal charge of lipoplexes ($|Q^*|_{max}$) obtained from eq 1, are shown for each lipoplex. Constant values of C = 2.78 10^{-14} (C^2/J) and q_{ren} = 5.45 10^{-18} C were used for the calculations.

System	$10^{15}Q_{ren}$ (C)	$10^{-15}S_0$ (part/L)	$10^{25}E_0$ (J)	$10^{18}\|Q^*\|_{max}$ (C)
DC-CHOL/DOPE-DNA α = 0.25	1.45	4.09	0.71	1.02
DC-CHOL/DOPE-DNA α = 1	2.53	1.68	9.21	5.02
DOEPC/DOPE-DNA α = 0.25	1.53	4.15	1.37	1.53
DOEPC/DOPE-DNA α = 0.5	2.07	2.20	4.83	3.23
DOEPC/DOPE-DNA α = 0.75	2.33	1.67	5.81	3.70
DOEPC/DOPE-DNA α = 1	2.46	1.37	4.36	3.25

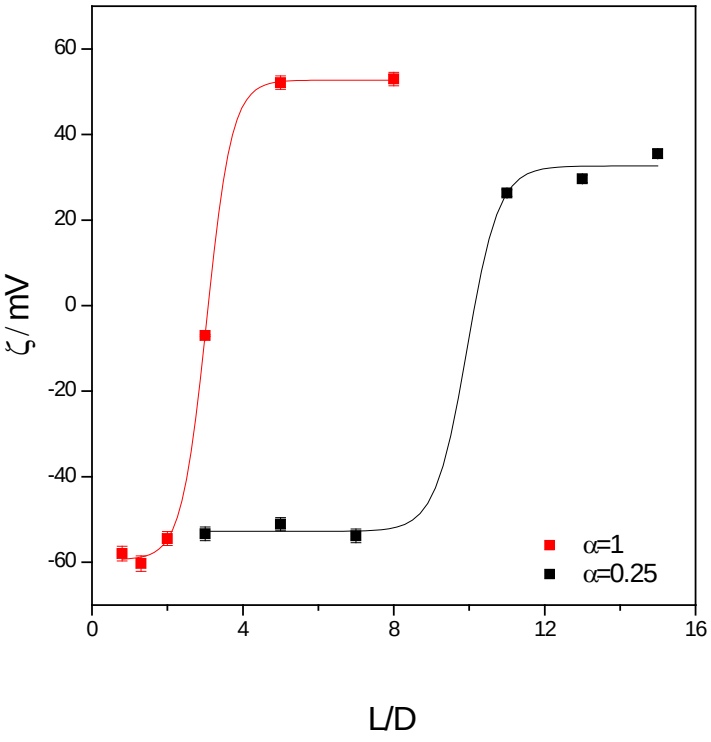

Figure 1

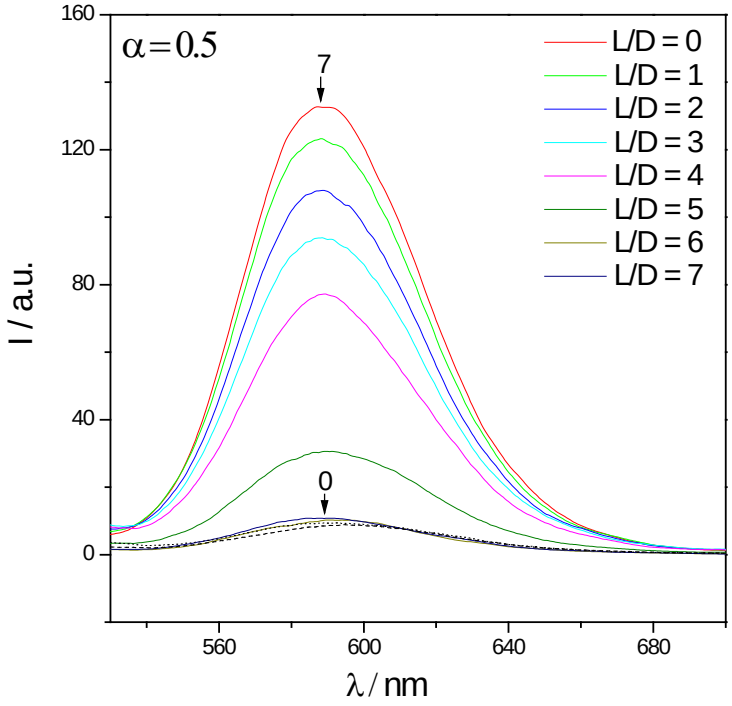
α = 0.5
7
0
L/D = 0
L/D = 1
L/D = 2
L/D = 3
L/D = 4
L/D = 5
L/D = 6
L/D = 7
I / a.u.
λ / nm
160
120
80
40
0
560
600
640
680

Figure 2

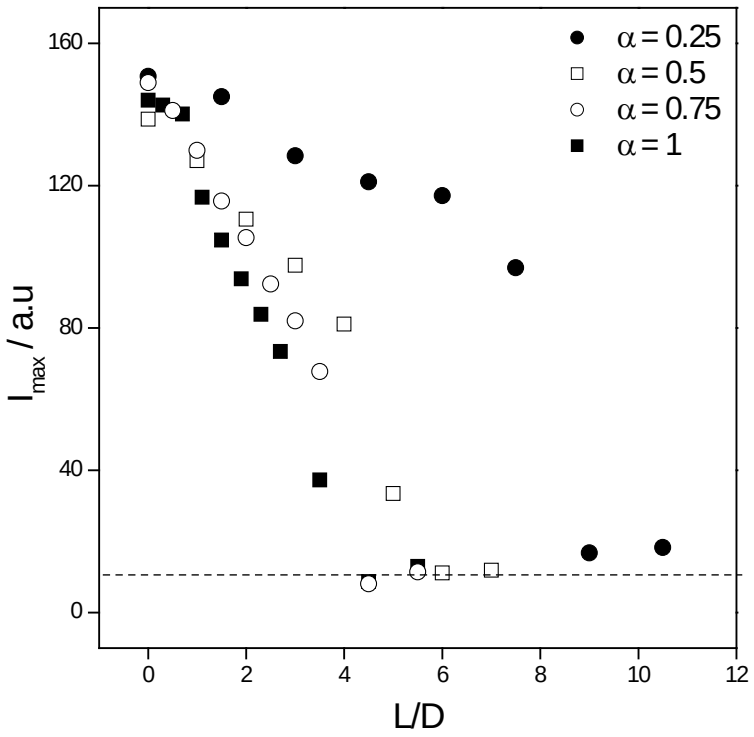

Figure 3

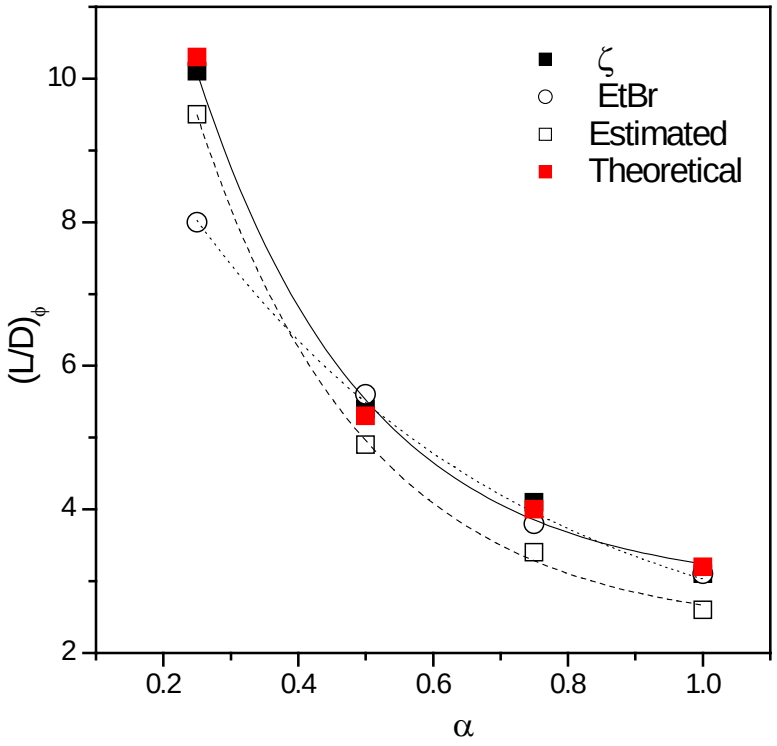

Figure 4

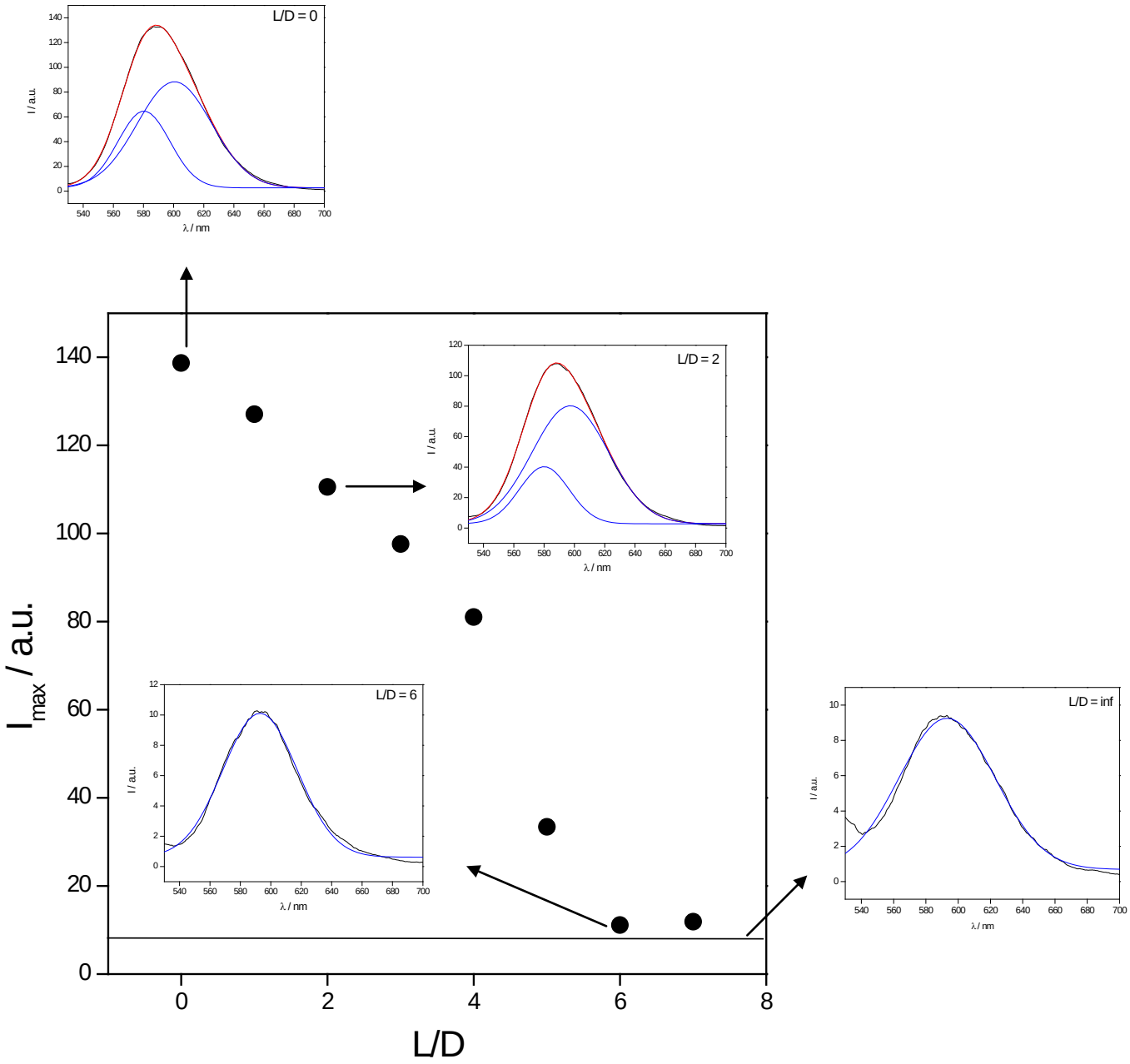

Figure 5

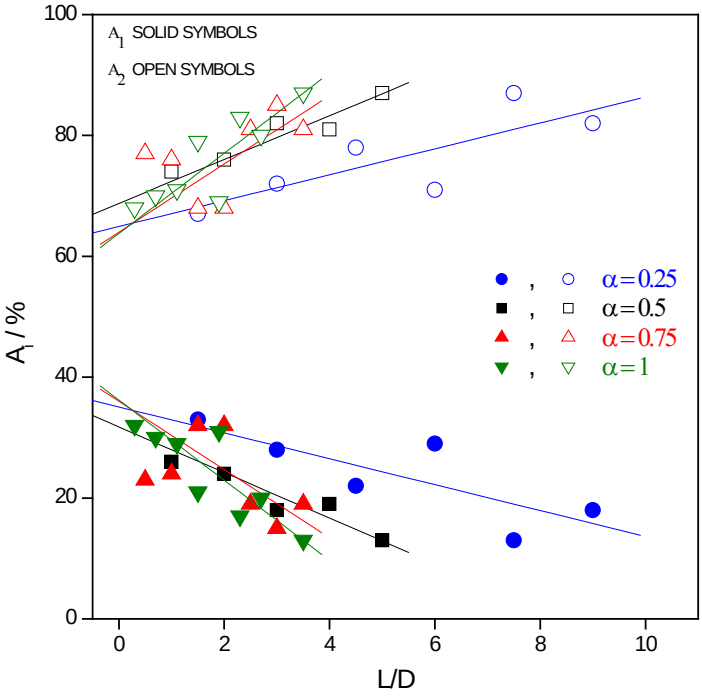
A1 SOLID SYMBOLS
A2 OPEN SYMBOLS
α=0.25
α=0.5
α=0.75
α=1
A1 / %
L/D
0
20
40
60
80
100
0
2
4
6
8
10

Figure 6

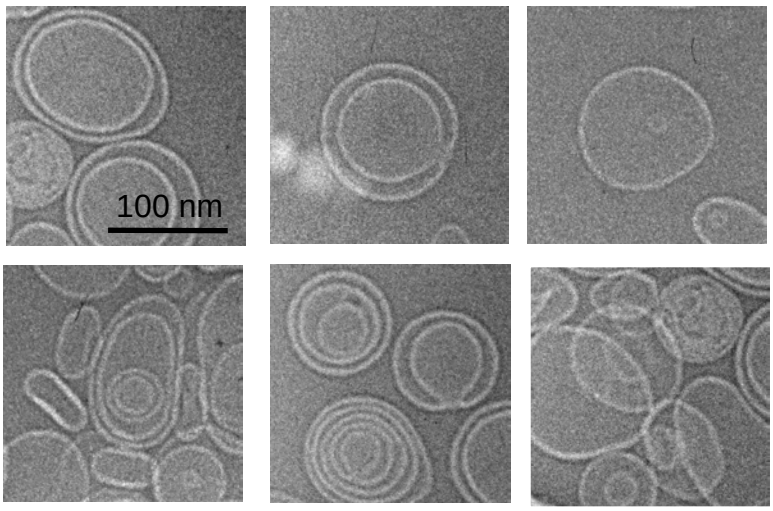

Figure 7

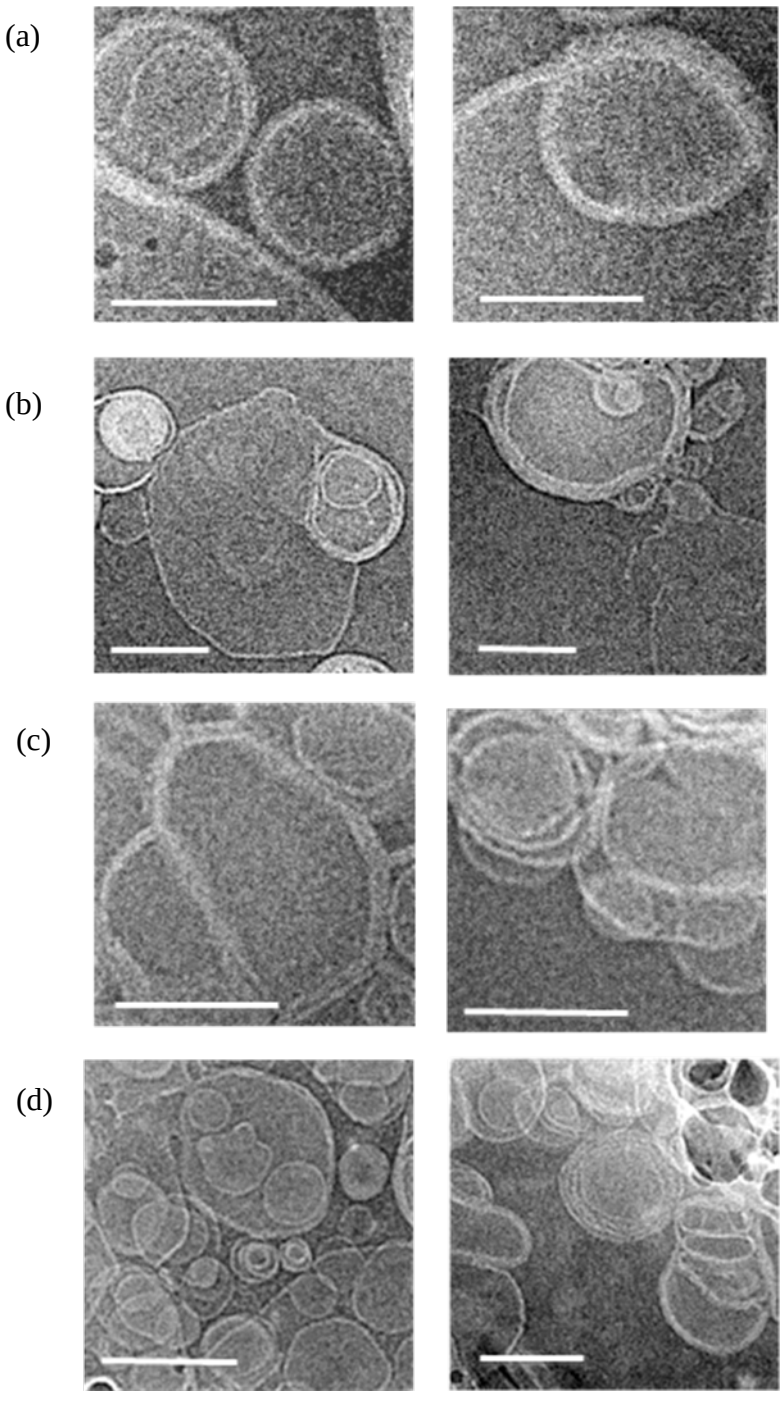

Figure 8

	A	B
α = 1 L/D = 8	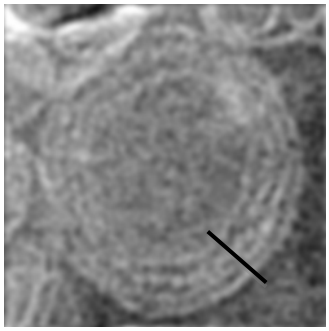	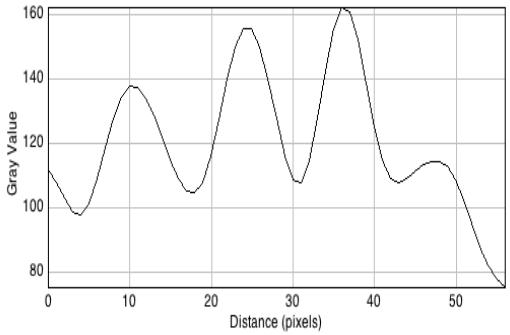
α = 0.75 L/D = 9	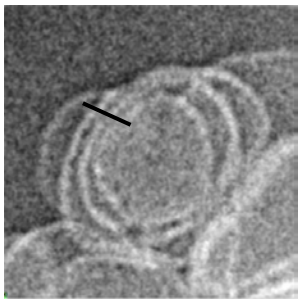	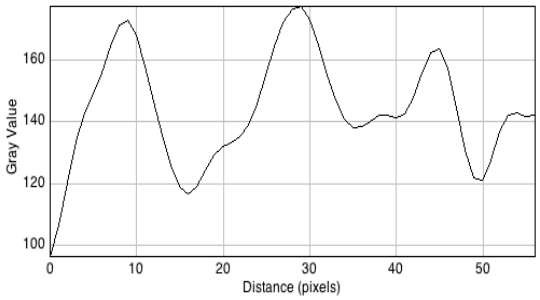
α = 0.5 L/D = 9	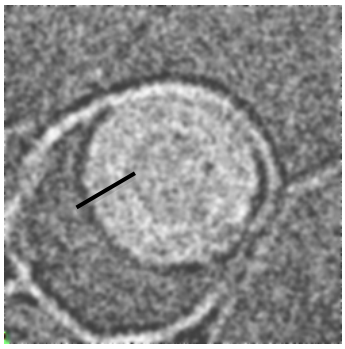	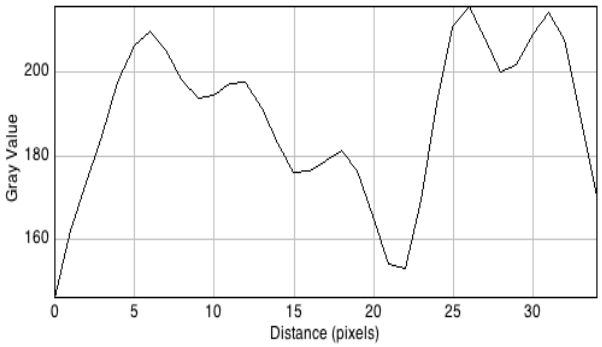

Figure 9

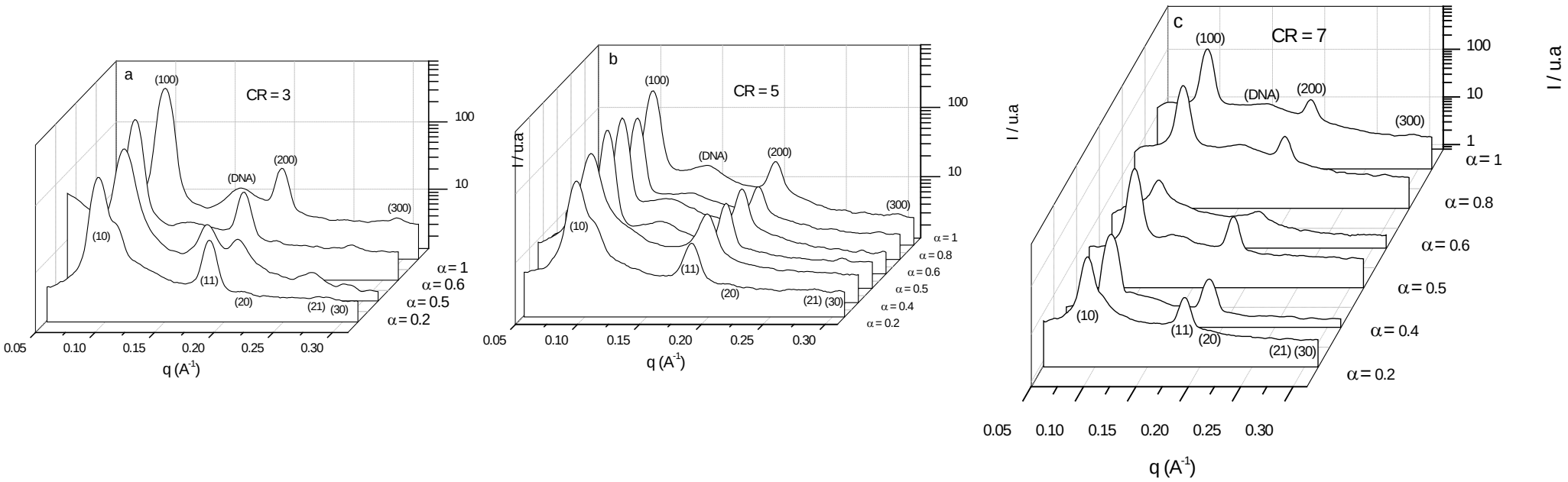
a
CR = 3
(100)
(DNA)
(200)
(300)
(10)
(11)
(20)
(21)
(30)
100
10
α = 1
α = 0.6
α = 0.5
α = 0.2
0.05
0.10
0.15
0.20
0.25
0.30
q (A-1)
b
CR = 5
I / u.a
α = 1
α = 0.8
α = 0.6
α = 0.5
α = 0.4
α = 0.2
c
CR = 7
I / u.a

Figure 10

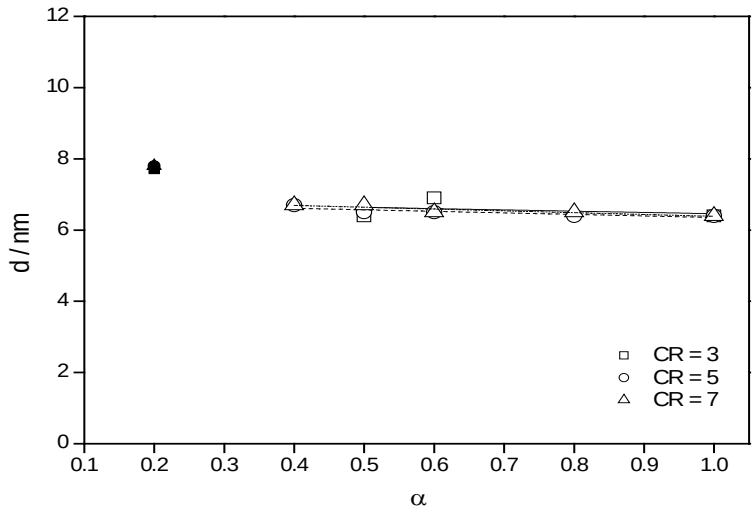

Figure 11

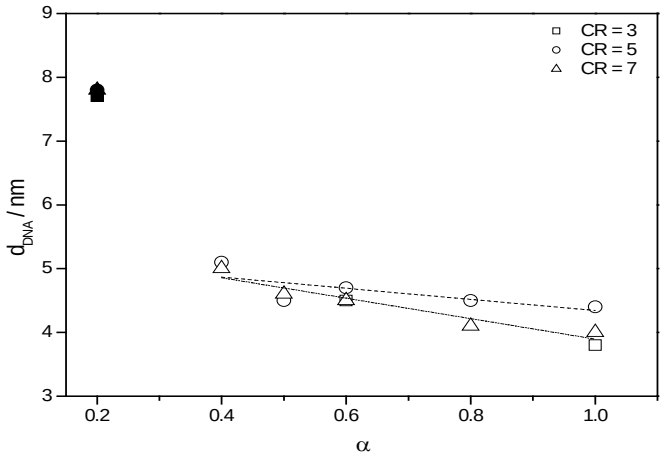

Figure 12

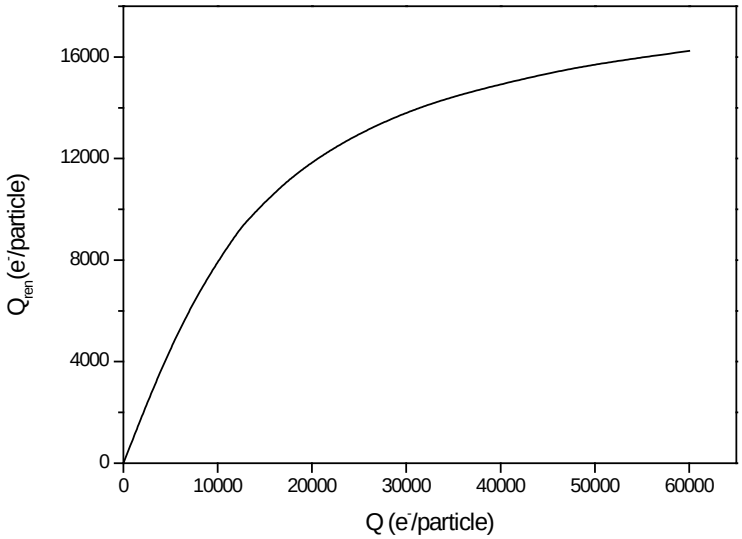
16000
12000
8000
4000
0
Q_{ren} (e^-/particle)
0
10000
20000
30000
40000
50000
60000
Q (e^-/particle)

Figure 13

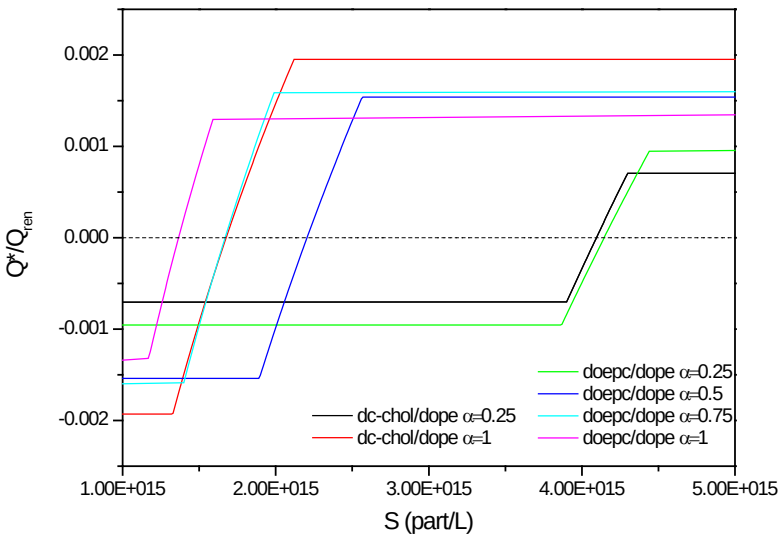
0.002
0.001
0.000
-0.001
-0.002
Q*/Q_en
1.00E+015
2.00E+015
3.00E+015
4.00E+015
5.00E+015
S (part/L)
dc-chol/dope α=0.25
dc-chol/dope α=1
doepc/dope α=0.25
doepc/dope α=0.5
doepc/dope α=0.75
doepc/dope α=1

Figure 14